Fuzzy Active Disturbance Rejection-Based Virtual Inertia Control Strategy for Wind Farms

Li, Tai; Wang, Yanbo; Su, Sunan; Qian, Huimin; Wang, Leqiu; Wang, Lei; Shen, Yanxia; Ji, Zhicheng

Published in:
Energies

DOI (link to publication from Publisher):
10.3390/en16103991

Publication date:
2023

Document Version
Publisher's PDF, also known as Version of record

energies

MDPI

Article

Fuzzy Active Disturbance Rejection-Based Virtual Inertia Control Strategy for Wind Farms

Tai Li [1], Yanbo Wang [2,*], Sunan Sun [3], Huimin Qian [3], Leqiu Wang [1], Lei Wang [1], Yanxia Shen [4] and Zhicheng Ji [4]

[1] School of Automation, Wuxi University, Wuxi 214105, China
[2] Department of Energy Technology, Aalborg University, 22222 Aalborg, Denmark
[3] College of Automation, Jiangsu University of Science and Technology, Zhenjiang 212003, China
[4] School of Internet of Things Engineering, Jiangnan University, Wuxi 214112, China
* Correspondence: ywa@et.aau.dk

Abstract: This paper presents an advanced virtual inertia control strategy for wind farms to provide transient power support in the presence of frequency events, where a fuzzy active disturbance rejection controller is developed to enable the operation of an energy storage system (ESS) so as to provide support for frequency regulation of the power grid. To effectively estimate the system frequency under uncertain noises, fuzzy rules are presented to adaptively tune the parameters of the extended state observer and to realize the power-sharing, to improve the anti-interference ability of the wind power system. Finally, simulation analysis in MATLAB/Simulink is provided to validate the effectiveness of the proposed control strategy. Simulation results show that the developed virtual inertia control strategy based on fuzzy active disturbance rejection control has a good inertia support capability. In addition, the proposed method is able to improve the anti-noise capability of the wind power system.

Keywords: wind farm; inertia support; fuzzy rules; active disturbance rejection control

Citation: Li, T.; Wang, Y.; Sun, S.; Qian, H.; Wang, L.; Wang, L.; Shen, Y.; Ji, Z. Fuzzy Active Disturbance Rejection-Based Virtual Inertia Control Strategy for Wind Farms. *Energies* **2023**, *16*, 3991. https://doi.org/10.3390/en16103991

Academic Editor: Surender Reddy Salkuti

Received: 18 December 2022
Revised: 7 April 2023
Accepted: 24 April 2023
Published: 9 May 2023

1. Introduction

With the rapid development of renewable energy technologies, power electronic converters have been increasingly adopted as efficient interfaces to integrate renewable energies into the power system. Unlike conventional synchronous generators that can support rotating inertia, the power converter-fed generators fail to provide rotating inertia inherently. Hence, the increasing adoption of power converter-interfaced generators tends to weaken the total rotating inertia of the power system so that the power system is subject to the intermittency and fluctuation of renewable energy sources [1,2]. Doubly fed induction generator (DFIG)-based wind turbines have been widely applied in modern wind power systems, where the stator of the DFIG is connected directly to the grid, and the rotor is connected to the grid by a back-to-back converter, as shown in Figure 1. The application of a back-to-back power converter decouples the wind generator from the power grid, which fails to respond automatically to frequency variations of the power system [3]. As the proportion of wind power generation increases, the influence of wind power generation on the operation performance of the power system is becoming evident. Hence, the grid codes pose new requirements for the grid support capability of wind turbines (WT) [4,5]. Inertia support of the wind power system is an important capability to respond automatically to the transient frequency events of the power system [6–8].

To increase the rotating inertia and support the transient frequency of a wind power plant in the presence of frequency events, inertia emulation strategies have been presented in previous works [9–16]. Inertia emulation methods mainly include rotor kinetic energy-based inertia emulation and energy storage (ES)-based inertia emulation. The authors of [9] designed a supplementary control loop to activate the kinetic energy of the wind generator in a DFIG-based wind power system, where the wind turbine may respond to

the frequency deviations that are similar to the inertia response of a synchronous generator. The authors of [10] compared two control strategies, including inertia and droop control. To utilize the rotating inertia of wind turbines, a kinetic energy-based inertial control strategy for a DFIG-based wind power plant was developed in [11], where DFIG contributed to transient frequency support by utilizing releasable kinetic energy, and the proposed kinetic energy-based gain scheme aims to activate the kinetic energy in the DFIG to boost the frequency nadir. Based on this, a data-driven virtual inertia control strategy was proposed in our previous work [12], where the noise interference in the frequency measurement process is effectively suppressed by designing the Riccati equation with a self-correction capability.

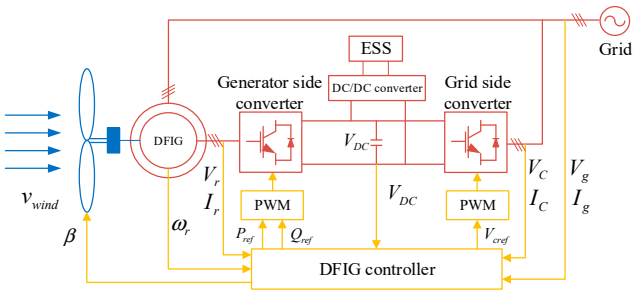

Figure 1. Diagram of a DFIG-based wind turbine.

Apart from the rotating inertia-based inertia emulation strategy, the energy storage (ES)-based inertia emulation method is also an effective solution to address the transient frequency disturbance. The virtual inertia control method based on the kinetic energy of the rotor realizes inertia support by releasing the kinetic energy stored in the generator rotor. Compared with the rotating energy-based inertia control strategy, the energy storage-based inertia control can suppress wind power fluctuations in a more flexible and effective manner through the rapid charge and discharge of the ES so as to address the fast power fluctuation.

In [13], the frequency control methods of wind turbine are reviewed, and requirements for ES devices to perform inertia emulation are analyzed. In [14], the requirements of the conventional kinetic energy-based inertia control strategies are analyzed by using the variable speed characteristics of variable speed wind turbine. Compared with the conventional kinetic energy-based inertia control strategies, the fuzzy theory-based control strategy is able to provide effective frequency support by predicting the frequency disturbance. In [15], an inertia control strategy based on fuzzy logic control (FLC) is developed to release the inertia energy of wind farm. According to the system frequency deviation, corresponding fuzzy rules are designed to dynamically provide the inertia support for power system. A fuzzy control-based inertia emulation strategy with ES device is presented in [16], where the fuzzy controller is employed to reduce the fluctuation of state-of-charge (SOC) and extend the lifespan of batteries. However, the WT is still affected by measurement noise. Therefore, it is important to improve the anti-interference ability of wind power system in the presence of grid frequency fluctuations.

In [17], an extended state observer (ESO) is developed to asymptotically estimate the aggregated disturbance that causes frequency deviation, so as to avoid measurement or calculation for system frequency derivation. In order to mitigate the rotor current disturbance caused by the change of electromagnetic torque, a maximum power point tracking (MPPT) control based on active disturbance rejection control (ADRC) is proposed in [18], which is able to effectively mitigate the rotor current disturbance. However, the existing virtual inertia control strategies fail to address the following drawbacks. (1) In the actual control process, PD virtual inertia is easy to operate, but PD parameters cannot be adjusted online, which results in poor control effect. (2) The frequency change rate of the power system is the basis of the entire inertia compensation control, but the frequency measured from wind turbine is interfered by a variety of local factors and measurement

noises, which can be caused by equipment parameter aging of measuring equipment and/or the difference in electromechanical properties between different equipments.

Therefore, this paper presents an adaptive inertia emulation strategy based on fuzzy logic auto-disturbance rejection control (FLC-ADRC), where fuzzy rules and the fuzzy active disturbance rejection control algorithm are introduced. The contributions of this work are explained as follows: (1) An inertia control method based on FLC-ADRC is proposed. (2) A nonlinear extended state observer is developed to predict the variation in frequency. (3) A fuzzy nonlinear control rate is used to adjust system parameters in the ESO online to improve the accuracy of FLC-ADRC. The rest of this paper is organized as follows: In Section 2, the traditional virtual inertia control strategies are reviewed. The proposed control strategy based on fuzzy logic auto-disturbance inertia control is developed in Section 3. In Section 4, the proposed control method is validated by simulation verification. Conclusions are drawn in Section 5.

2. System Description and Problem Formulation

2.1. System Description

A simplified diagram of a DFIG-based wind turbine is shown in Figure 1, where the stator is connected directly to the grid, and the rotor is connected to the grid by a back-to-back converter. The back-to-back converter decouples the wind turbine from the power grid. The control system enables the power converter to perform the following tasks: (1) Maximum power point tracking is implemented when the wind speed is below the rated wind speed. (2) The DC-link voltage of the power converter is maintained. (3) Reactive power support is provided in the presence of a grid fault. The mechanical power extracted from the wind turbine is given as Formula (1) [19].

$$P_m = 0.5\pi\rho R^2 C_p(\lambda, \beta)v^3 \tag{1}$$

where P_m is the mechanical power extracted from the wind energy, ρ = 1.22 kg/m^3 is the air density in kilograms per cubic meter, R is the turbine radius, ω is the turbine angular speed, v is the wind speed, $\lambda = \omega R/v$ is the blade top speed ratio; β is the blade pitch angle, $C_p(\lambda,\beta)$ is the power performance coefficient of the wind turbine, which is related to the blade pitch angle and the blade tip speed ratio.

2.2. Traditional Virtual Inertial Controller

Figure 2 shows the inertia control structure of the additional power outer loop. Two parts are included in the outer power loop, where the dynamic frequency deviation (Δf) is enacted by the proportional part, and the frequency deviation change rate (df/dt) is enacted by the differential part. When a power imbalance in the grid happens, the system frequency responds quickly, and the differential part is crucial at this point. When the system frequency fluctuation happens, the proportional part will be crucial. The active power compensation of the DFIG can be represented as Formula (2).

$$P_{VRB} = K_d \frac{d\Delta f}{dt} + K_p \Delta f \tag{2}$$

where P_{VRB}, K_d, K_p, Δf, and df/dt are the targeted inertia power, the differential parameter, the proportion parameter, the frequency offset, and the frequency rate, respectively. The inertia response of the synchronous generator is simulated through the ESSs, which are used to increase the equivalent inertia of the power system in order to improve the transient performance of the system frequency. The inertia response of the power system [20] is represented as Formula (3).

$$\Delta P_{VRB} = 2H \frac{d\Delta f}{dt} + D\Delta f \tag{3}$$

where H is the inertia time constant, and D is the damping coefficient. The inertia response of the WT can be given as Formula (4).

$$\Delta P_{VRB} = (2H + K_d)\frac{d\Delta f}{dt} + (D + K_p)\Delta f \tag{4}$$

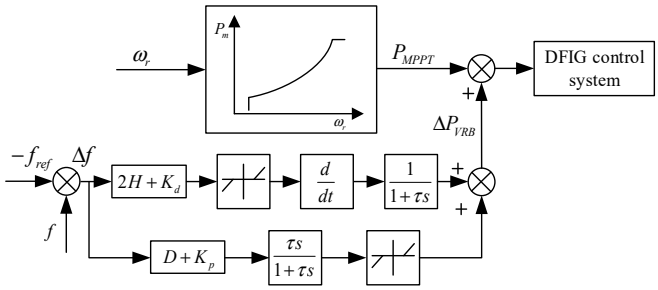

Figure 2. Inertia control structure of the additional power outer loop.

The PD-based virtual inertia strategy can be performed in practical operations easily. However, this method is subject to external interference, which fails to provide sufficient inertia support based on the specific conditions of the actual wind power system. The uncertainty of the DFIG-inertial simulation system is caused by the measurement noise in the process of power grid frequency measurements. Therefore, it is urgent to develop a method to improve the anti-interference ability of the system and the virtual inertia control effect. To address this issue, this paper presents an inertia control strategy based on a fuzzy logic active disturbance rejection control (FLC-ADRC) strategy for inertia emulation control.

3. The Proposed Inertia Control Strategy Based on FLC-ADRC

In this section, the FLC-ADRC strategy is developed to perform inertia emulation. Figure 3 shows the simplified diagram of the FLC-ADRC-based inertia control method. FLC-ADRC was composed of a fuzzy controller and an auto disturbance rejection controller (ADRC). The ADRC was a nonlinear PID controller with good adaptability and robustness, and fuzzy logic was introduced to adaptively tune the parameters of ADRC. In this proposed FLC-ADRC, the ESO was adopted to estimate the frequency change rate of the inertia control system. The external disturbance and unknown measurement noise were estimated as the extended state of the ESO, where the observer parameters were adaptively adjusted online by fuzzy rules.

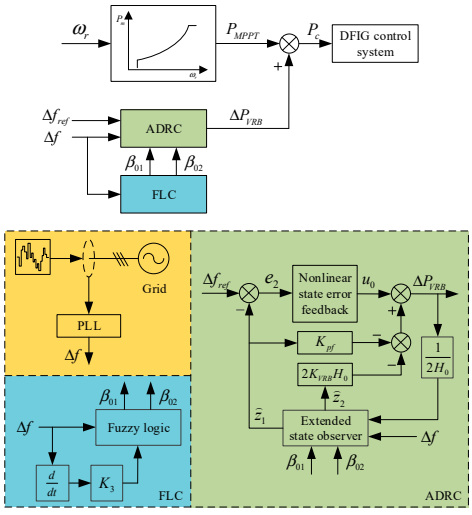

Figure 3. Simplified diagram of the fuzzy ADRC-based inertia emulation method.

3.1. Fuzzy Active Disturbance Rejection Controller

3.1.1. Extended State Observer

The frequency dynamic response can be given as Formula (5).

$$2H\frac{d\Delta f}{dt} = -D\Delta f + \Delta P_G + \Delta P_{VRB} + \Delta P_T - \Delta P_L \tag{5}$$

where P_G is the power provided by conventional synchronous generators, P_{VRB} is the reference value of the active power increment produced by the energy storage virtual inertia control, and P_T is the exchange power between adjacent systems. P_L is the active load distribution of the system, and ΔP_G, ΔP_{VRB}, ΔP_T, and ΔP_L are the increments of P_G, P_{VRB}, P_T, and P_L, respectively.

The first-order representation can be given as Formula (6) by Formula (5).

$$\frac{d\Delta f}{dt} = \frac{1}{2H}\Delta P_{VRB} + \frac{1}{2H}(-D\Delta f + \Delta P_G + \Delta P_T - \Delta P_L) \tag{6}$$

Formula (6) can be rewritten as Formula (7).

$$\begin{aligned}\tfrac{d\Delta f}{dt} = \tfrac{1}{2H_0}\Delta P_{VRB} + [\tfrac{1}{2H}(-D\Delta f + \Delta P_G + \Delta P_T - \Delta P_L)\\ +(\tfrac{1}{2H} - \tfrac{1}{2H_0})\Delta P_{VRB}]\end{aligned} \tag{7}$$

Taking the following equation into Formula (7).

$$a(t) = \frac{1}{2H}(-D\Delta f + \Delta P_G + \Delta P_T - \Delta P_L) + (\frac{1}{2H} - \frac{1}{2H_0})\Delta P_{VRB}$$

Formula (7) can be rewritten as Formula (8).

$$\frac{d\Delta f}{dt} = a(t) + \frac{1}{2H_0}\Delta P_{VRB} \tag{8}$$

where *a(t)* is all the interference of the total active power imbalance (excluding ESS) on the frequency rate.

According to Formula (8), the state variable $x = \Delta f$ and the control input $u = \Delta P_{VRB}$ are defined, and the unknown total disturbance of the system *a(t)*, the system model is represented as Formula (9).

$$\begin{cases} \dot{x} = a(t) + \frac{1}{2H_0}u \\ y = x \end{cases} \tag{9}$$

According to Formula (11), ESO can be used to estimate the state variables x and the newly expanded state variables *a(t)*. Therefore, the new state variables $z_1 = x$, $z_2 = a(t)$, the output $y = z_1 = x$, and ESO can be represented as Formula (10).

$$\begin{cases} e_1 = z_1 - \widehat{z}_1 \\ \dot{\widehat{z}}_1 = \widehat{z}_2 + \frac{1}{2H_0}u - \beta_{01}e_1 \\ \dot{\widehat{z}}_2 = -\beta_{02}fal(e_1, \alpha_1, \delta_1) \end{cases} \tag{10}$$

where $\widehat{z}_1$ is the observed state of z_1, $\widehat{z}_2$ is the observed state of z_2, $\dot{\widehat{z}}_1$ and $\dot{\widehat{z}}_2$ represent the derivative of $\widehat{z}_1$ and $\widehat{z}_2$, e_1 is the observer error, α_1 is a nonlinear factor related to the control accuracy, Δ_1 is the filtering factor (choosing appropriate parameters can avoid the occurrence of high-frequency oscillations), u is the control input, $\beta_{01,}$ and β_{02} are the

adjustable gain parameters. The function *fal*(e_1,α_1,Δ_1) has fast convergence and a certain filtering effect, which can be represented as Formula (11).

$$fal(e_1, \alpha_1, \delta_1) = \begin{cases} \frac{e_1}{\delta_1^{1-\alpha}} & |e_1| \le \delta_1 \\ |e_1|^{\alpha_1} sign(e_1) & |e_1| > \delta_1 \end{cases} \tag{11}$$

Therefore, if the parameters β_{01} and β_{02} are selected reasonably, the observation $\widehat{z}_1$ of the ESO output, shown in Equation (12), will approach x, which is the system offset Δf. To respond to frequency derivation, the ES-based virtual inertia control strategy is developed as Formula (12).

$$\Delta P_{VRB} \approx -\frac{K_{VRB}}{1 - K_{VRB}} 2H_0 \frac{d\Delta f}{dt} = -K_{VRB} \cdot 2H_0 \widehat{z}_2 \tag{12}$$

where K_{VRB} is the inertia response participation coefficient of ESS, and the value range is $0 \le K_{VRB} \le 1$.

When adding the reference power increment of the synchronous generator's primary frequency modulation, Formula (12) is rewritten as Formula (13).

$$\Delta P_{VRB} = -K_{VRB} \cdot 2H_0 \widehat{z}_2 - K_{pf} \widehat{z}_1 \tag{13}$$

where K_{pf} is the equivalent frequency adjustment effect coefficient. This formula simulates the inertia response and primary frequency control ability of synchronous wind generators.

3.1.2. Nonlinear State Feedback Controller

The control objective of ADRC is to make z_1 tend to zero; that is, the system frequency deviation is zero. Therefore, the control quantity u in Formula (9) can be taken as:

$$\begin{cases} u = u_0 + \Delta P_{VRB} \\ u_0 = \beta_{03} \Delta f_{ref} - z_1 \end{cases} \tag{14}$$

Formula (14) is the nonlinear feedback control law of the ADRC designed in this chapter. Therefore, the approximate mathematical model of ADRC designed in this chapter is shown in Formula (15):

$$\begin{cases} \Delta f = 0 \\ z_1 = x \\ z_2 = a(t) \\ e_1 = z_1 - \widehat{z}_1 \\ \dot{\widehat{z}}_1 = \widehat{z}_2 + \frac{1}{2H_0} u - \beta_{01} e_1 \\ \dot{\widehat{z}}_2 = -\beta_{02} fal(e_1, \alpha_1, \delta_1) \\ u = u_0 + \Delta P_{VRB} \\ u_0 = \beta_{03} \Delta f_{ref} - z_1 \end{cases} \tag{15}$$

3.1.3. Fuzzy Rules

In the process of DFIG participating in grid frequency regulation, fuzzy control has better robustness and the anti-interference ability for a nonlinear and complex time-varying wind power system. In this part, fuzzy rules are used to tune the parameters of an active disturbance rejection controller online to realize adaptive control. The operation performance of ADRC mainly depends on the internal parameters of the controller. To adaptively adjust the internal parameters of the controller, fuzzy rules were adopted to adjust the parameters of ADRC online to realize the adaptive control. To meet the self-tuning requirements of e_2 and e_3 (the change rate of e_2) to β_{01} and β_{02} at different times, e_2

and e_3 were used as fuzzy input variables. Fuzzy rules were used to adaptively modify parameters β_{01} and β_{02} online. Among them, when the Δf and $d\Delta f/dt$ changed, β_{01} was positively correlated with the two inputs of the fuzzy logic controller, while β_{02} was negatively correlated with it, and the corresponding virtual inertia control effect of energy storage compensation was obtained. According to experimental data, the ranges of e_2 and e_3 were $[-0.3, 0.3]$ and $[-3, 3]$, respectively. The domains of output variables β_{01} and β_{02} of the fuzzy controller were [4, 6] and [0.001, 0.01], respectively. Among them, β_{01} and β_{02} were the outputs of the fuzzy rules, and the fuzzy subsets of e_2, β_{01}, and β_{02} were defined as {NB, NS, ZO, PS, PB}. The fuzzy subsets of e_3 were defined as {NB, ZO, PB}. The corresponding membership function is shown in Figure 4.

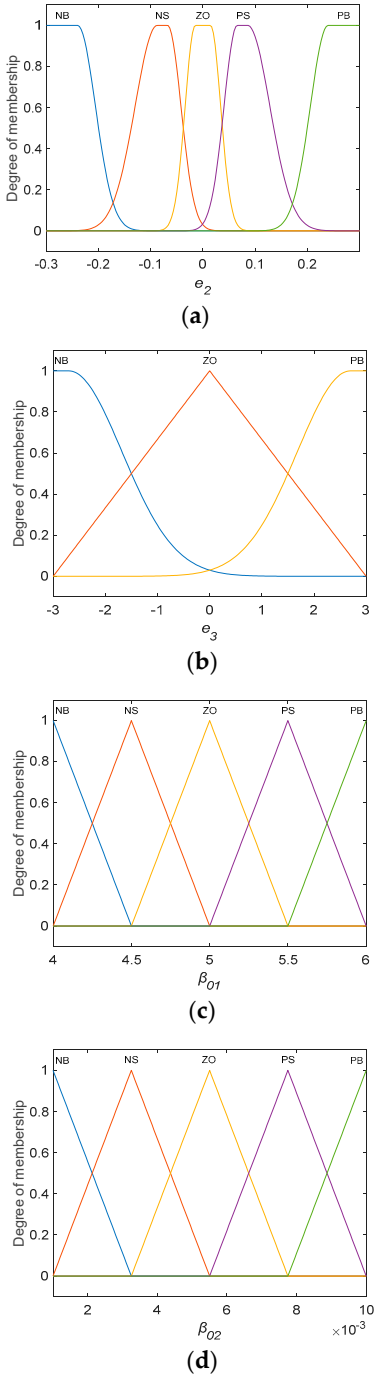

Figure 4. Membership function of e_2, e_3, β_{01} and β_{02}. (**a**) Membership function of e_2, (**b**) Membership function of e_3, (**c**) Membership function of β_{01}, and (**d**) Membership function of β_{02}.

The fuzzy roles of β_{01} and β_{02} are defined in Table 1. According to the membership table of each fuzzy subset and the fuzzy control model of each parameter, the fuzzy matrix table specified by fuzzy synthetic reasoning was used.

Table 1. Fuzzy roles of β01 and β0.

e_2	e_3		
	NB	**ZO**	**PB**
NB	NB/PB	NS/PS	ZO/ZO
NS	NB/PS	NS/PS	PS/NS
ZO	NS/PS	ZO/ZO	PS/NS
PS	NS/PS	PS/NS	PB/NS
PB	ZO/ZO	PS/NS	PB/NS

The fuzzy rules were specified according to the frequency change rate. Then, fuzzy rules were used to modify ESO parameters β_{01} and β_{02} online. The reasoning principle embodied in the controller was that when the Δf and the $d\Delta f/dt$ were negative, the output β_{01} was negative, and the output β_{02} was positive to reduce system frequency fluctuation. When the Δf and the $d\Delta f/dt$ were positive, the output β_{01} was positive, and the output β_{02} was negative to speed up system frequency recovery. The controller adjusted the output power of ESS in real-time according to the variation in the system frequency and effectively compensated the virtual inertia of the wind power system. The output surface of the fuzzy controller is shown in Figure 5.

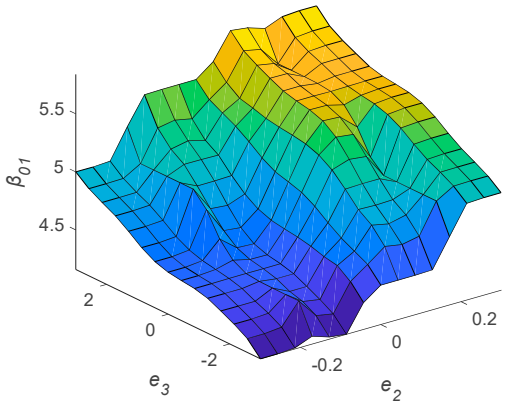

(**a**)

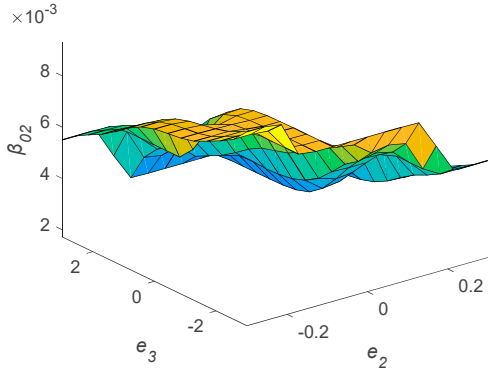

(**b**)

Figure 5. Output surface. (**a**) β_{01} surface and (**b**) β_{02} surface.

4. Simulation Verification

To validate the effectiveness of the proposed FLC-ADRC-based virtual inertia control strategy, simulation verification was performed in MATLAB/Simulink. Figure 6 shows the single-line diagram of the exemplified system. The wind power system included six 1.5 MW DFIG-based wind turbines, where each generator was equipped with an ESS with a capacity of 250 kW, and the rated power of the equivalent synchronous generator in the power grid was 120 MW. An energy storage system was connected by a DC/DC converter, and the FLC-ADRC controller was designed to control the DC/DC converter so as to provide active power support for the energy storage system. The related parameters of the wind power system are given in Table 2.

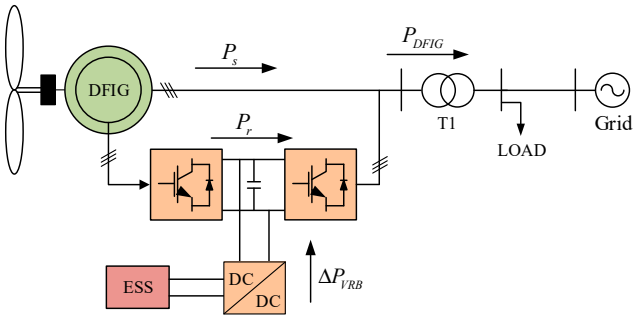

Figure 6. Simplified diagram of the exemplified system.

Table 2. System Parameters of Wind Power System.

Parameter	Value
Wind farm rated power	9 MW
DFIG unit rated power, P_{nom}	1.5 MW
DFIG rated voltage, V_{nom}	575 V
Air density, ρ	1.22 kg/m^3
Turbine radius, R	35.25 m
Inertia of generator, H_g	0.62 s
Inertia of wind turbine, H_{WT}	4.33 s
Magnetizing inductance, L_m	2.9036 (p.u.)
Stator self-inductance, L_s	0.1714 (p.u.)
Rotor self-inductance, L_r	0.1563 (p.u.)
Cut in wind speed, v_c	3 m/s
Cut out wind speed, v_o	25 m/s
Rated wind speed, v_r	11 m/s

It is important for the inertia support ability of a wind turbine to reduce the frequency change rate of the system when frequency events occur. Then, in the condition of an 11 m/s wind speed, the simulation of the proposed control method was studied. The capability of transient inertia support under three different conditions was recorded, including frequency decrease or increase. In order to verify the correctness of the proposed control method, the comparative analysis is performed to the frequency regulation under three different situations.

PD Inertia Control: Transient inertia support was provided to DFIG, that operated with PD-based inertia control. ADRC inertia control: Transient inertia support was provided to the DFIG, which was operated with ADRC-based inertia control. FLC-ADRC inertia control: Transient inertia support was provided to the DFIG, which operated with FLC-ADRC-based inertia control.

4.1. Case I: Frequency Decrease

When the system frequency deviation was more than 0.03 Hz, the proposed virtual inertia control method engaged. Figures 7–10 show the operation performance of the wind power system under different control methods when the system frequency decreased.

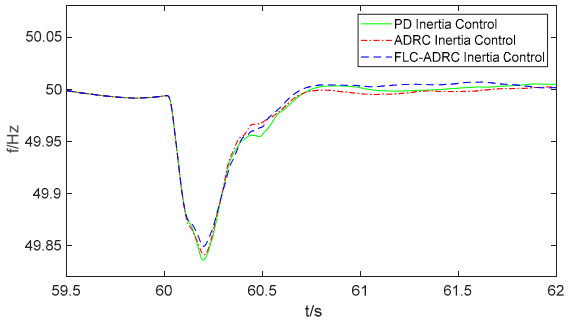

Figure 7. Simulation results for grid frequency.

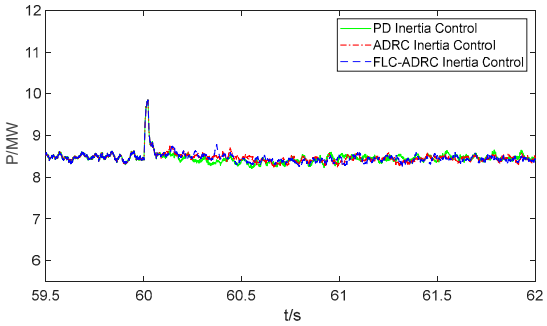

Figure 8. Simulation results for active power.

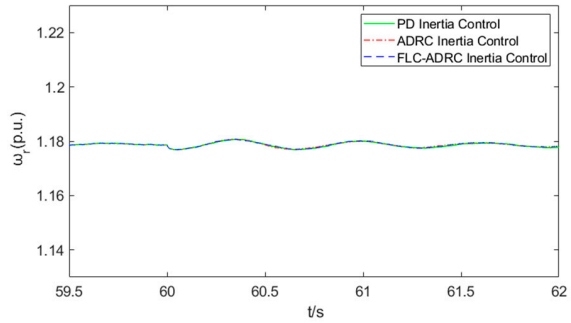

Figure 9. Simulation results for DFIG rotor speed.

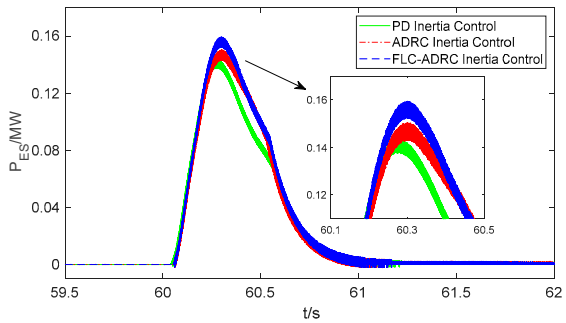

Figure 10. Simulation results for the output power of the ESS.

Figure 7 shows the simulation results for grid frequency when the system frequency was decreased under several methods of control. It can be observed that the system

frequency dropped from 49.99 Hz to 49.82 Hz under traditional PD inertia control. If the ADRC-based inertia control method was activated, the system frequency dropped from 50.00 Hz to 49.83 Hz. Compared with the traditional virtual inertia control strategy, the frequency nadir increased by 0.2%. Once the FLC-ADRC-based control method was activated, the system frequency dropped from 50.00 Hz to 49.85 Hz, and the frequency nadir increased by 0.6%.

Figure 8 shows the simulation results about active power response once the PD inertia control, ADRC inertia control, and FLC-ADRC inertia control were activated at 60 s. This is because the inertia control methods based on the ESS provide inertial support for the power system by releasing ESS energy.

Figure 9 shows the simulation results for DFIG rotor speed under several methods of control when the system frequency was decreased. It is evident that the rotor speed did not decrease under different inertia control methods at 60 s since the ES-based inertia emulation method provided inertia support.

Figure 10 shows simulation results for the output power of ESS when the system frequency was decreased under several methods of control. It is evident that the power released by traditional PD inertia control, ADRC inertia control, and FLC-ADRC inertia control increased, and the FLC-ADRC-based control method provided frequency support with higher inertia power. Simulation results showed that traditional PD inertia control effectively suppressed the frequency drop by releasing the energy of the ES when the system frequency decreased. Compared with traditional PD inertia control, ADRC inertia control reduced the peak value of the frequency drop. The improved FLC-ADRC control method based on ADRC made the control effect more obvious, and the activation and exit speed of the energy storage device was faster. Therefore, the proposed FLC-ADRC inertia control method can provide better inertia support by releasing the energy of the ESS.

4.2. Case II: Frequency Increase

When the system frequency deviation was more than 0.03 Hz, the proposed virtual inertia control method engaged. Figures 11–14 show the operating performance of the wind power system in which the system frequency was increased under several methods of control.

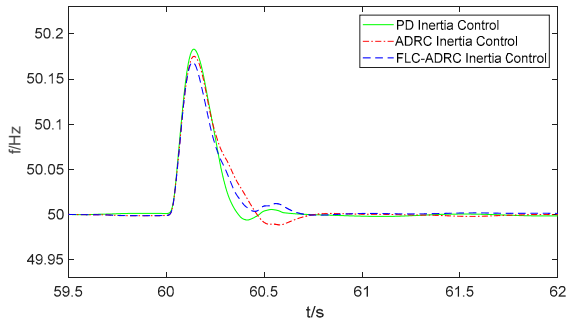

Figure 11. Simulation results for grid frequency.

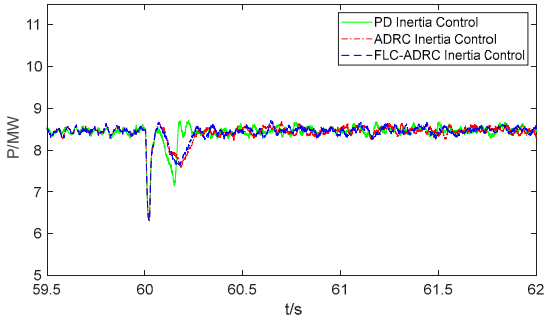

Figure 12. Simulation results for active power.

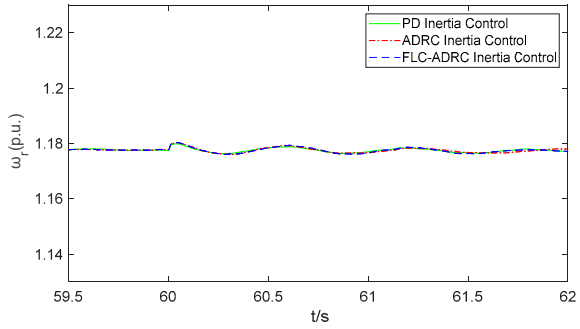

Figure 13. Simulation results for DFIG rotor speed.

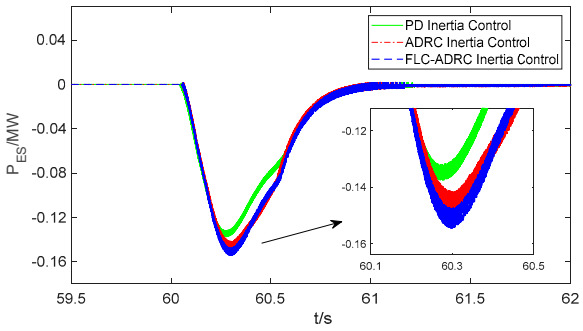

Figure 14. Simulation results for output power of ESS.

Figure 11 shows the simulation results for grid frequency under several methods of control when the system frequency was increased. It is evident that the system frequency rose from 50.00 Hz to 50.18 Hz under traditional inertia control of the PD. If the inertia control method ADRC-based was activated, the system frequency rose from 50.00 Hz to 50.17 Hz. Compared with the traditional virtual inertia control strategy, the frequency zenith was reduced by 0.2%. Once the FLC-ADRC-based control method was activated, the system frequency rose from 50.00 Hz to 50.15 Hz, and the frequency zenith was reduced by 0.6%.

Figure 12 shows the simulation results for the active power response of the DFIG under several methods of control when the system frequency was increased. It is evident that the response of active power was observed once the PD inertia control, ADRC inertia control, and FLC-ADRC inertia control were activated at 60 s since the inertia control method based on ESS realized inertia support by a charging operation of the ESS.

Figure 13 shows the simulation results of DFIG rotor speed under several methods of control when the system frequency was increased. It is evident that the rotor speed did not change significantly under different inertia control methods at 60 s since the ES-based inertia emulation method realized inertia support.

Figure 14 shows the simulation results for the output power of the ESS under several methods of control when the system frequency increased. It can be seen that the power absorbed by traditional PD inertia control, ADRC inertia control, and FLC-ADRC inertia control increased, and the FLC-ADRC-based control method realized frequency support with higher inertia power.

Simulation results showed that traditional PD inertia control effectively suppressed the frequency increase by charging the ES energy when the system frequency was increased. Compared with traditional PD inertia control, ADRC inertia control reduced the peak value and speed of frequency variation. The improved FLC-ADRC control method based on ADRC made the control effect more obvious. Therefore, the proposed FLC-ADRC control method can implement better inertia support for the power grid.

4.3. Case III: Frequency Decrease with Measurement Noise

In this case, the measurement noises were considered, where white noise with a standard deviation of ±0.02 Hz was given to emulate the influence of frequency measurement noise. It can be seen that the effect of FLC-ADRC was better than that of ADRC. Thus, the ADRC inertia control method is not related for this case. The PD inertia control method and the proposed virtual inertia control method were not activated unless the system frequency deviation was more than 0.03 Hz. Figures 15–18 show the operating performance of the wind power system under different control methods when the system frequency was decreased with measurement noise.

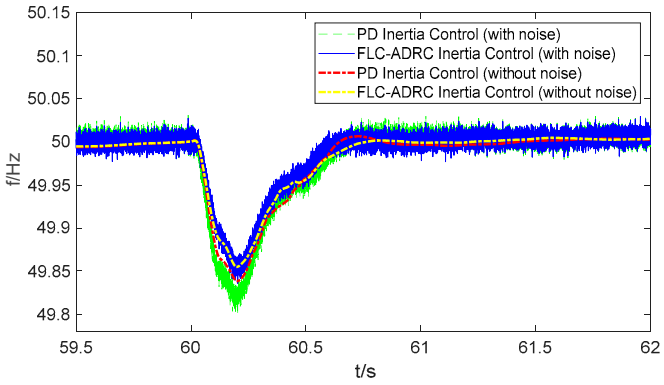

Figure 15. Simulation results for grid frequency considering measurement noise of control system.

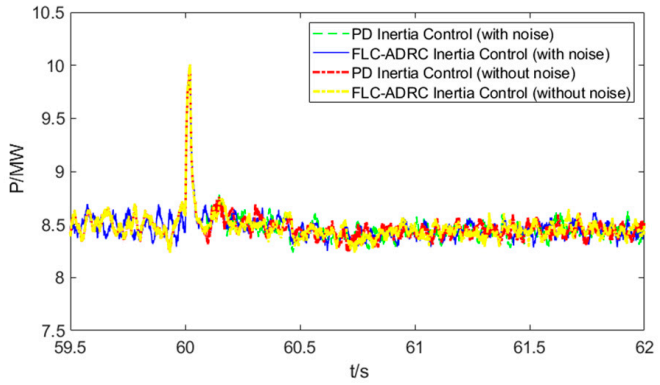

Figure 16. Simulation results for active power considering measurement noise of control system.

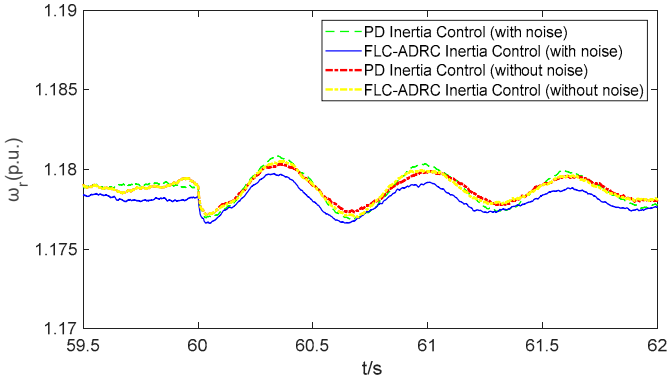

Figure 17. Simulation results for DFIG rotor speed considering measurement noise of control system.

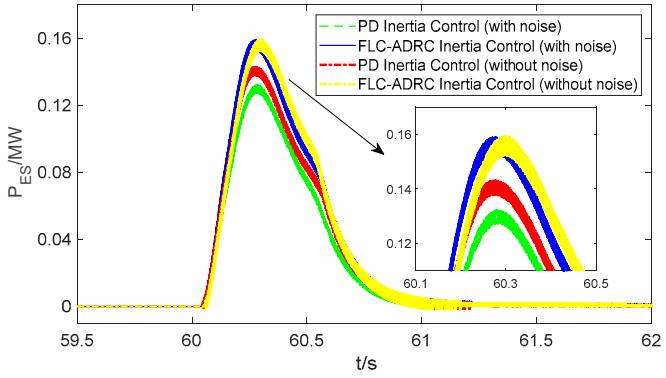

Figure 18. Simulation results for output power of the ESS considering measurement noise of the control system.

Figure 15 shows the grid frequency considering the measurement noise of the control system when the system frequency was decreased. It is evident that in the absence of noise, the system frequency was reduced from 50.00 Hz to 49.84 Hz under traditional PD inertia control. However, when the system frequency decreased with measurement noise, the measurement noise dramatically affected the PD inertia control performance that, brought about a system frequency fluctuation of 50.00 Hz to 49.80 Hz with obvious glitches. However, the performance of FLC-ADRC inertia control was less affected by the noise situation. In the absence of noise, the system frequency was reduced from 50.00 Hz to 49.85 Hz under FLC-ADRC virtual inertia control. When the system frequency decreased with measurement noise, the situation affected the performance of the FLC-ADRC inertia control less and induced a system frequency fluctuation of 50.00 Hz to 49.83 Hz with glitches. After the FLC-ADRC inertia control method was activated, compared with the case without noise signal, the frequency nadir was similar to measurement noise.

Figure 16 shows the active power considering the measurement noise of the control system when the system frequency was decreased. It is evident that the response of active power was observed once the PD inertia control and FLC-ADRC inertia control were activated at 60 s since the ES-based inertia control method provided inertia support by releasing the stored energy.

Figure 17 shows the DFIG rotor speed considering the measurement noise of the control system when the system frequency was decreased. It is evident that the rotor speed did not decrease under different inertia control methods at 60 s since the ES-based inertia emulation method provided inertia support.

Figure 18 shows the output power of the ESS considering the measurement noise of the control system when the system frequency decreased. When the system had an absence of measurement noise, the output power of the ESS under the FLC-ADRC virtual inertia control method was more than the output power under the PD inertia control in the absence of measurement noise. When the system had measurement noise, compared with the traditional inertia control of the PD method, the FLC-ADRC inertial control method better released the output power provided by the ESS.

Simulation results showed that the proposed FLC-ADRC inertia control method improved the anti-noise performance of the system when the system frequency was decreased with the measurement noise.

5. Conclusions

The power converter-interfaced wind turbine fails to inherently provide inertia support due to the decoupling of the wind generator and the power grid. This paper presented an FLC-ADRC-based inertia control strategy for a wind farm. The design guidelines of the ADRC controller were first established for a wind turbine to perform inertia support. Then, fuzzy rules were integrated into the ADRC controller. An extended state observer was adopted to estimate the rate of change in the system frequency in this FLC-ADRC controller,

which was able to effectively address the interference from noise in the measurement of the rate of frequency change. The simulation results showed that the proposed FLC-ADRC method improved the operational performance of the inertia control system and improved the interference rejection capability against external disturbance and measurement noises.

Author Contributions: Conceptualization, T.L. and Y.W.; Methodology, T.L., S.S. and H.Q.; Validation, L.W. (Leqiu Wang); Writing-original draft preparation, T.L.; Writing-review and editing, Y.W., L.W. (Lei Wang), Y.S. and Z.J.; Supervision, Y.S. and Z.J. All authors have read and agreed to the published version of the manuscript.

Funding: This study is supported by the State Key Laboratory of Alternate Electrical Power System with Renewable Energy Sources (Grant NO. LAPS21021).

Institutional Review Board Statement: Not applicable.

Informed Consent Statement: Not applicable.

Data Availability Statement: No new data were created.

Conflicts of Interest: The authors declare no conflict of interest.

References

1. Li, Y.J.; Xu, Z.; Wong, K.P. Advanced Control Strategies of PMSG-Based Wind Turbines for System Inertia Support. *IEEE Trans. Power Syst.* **2016**, *32*, 3027–3037. [CrossRef]
2. Wang, Y.B.; Wang, X.F.; Chen, T.; Blaabjerg, F. Small-Signal Stability Analysis of Inverter-Fed Power Systems Using Component Connection Method. *IEEE Trans. Smart Grid.* **2018**, *9*, 5301–5310. [CrossRef]
3. Ye, H.; Pei, W.; Qi, Z.P. Analytical Modeling of Inertial and Droop Responses from a Wind Farm for Short-term Frequency Regulation in Power Systems. *IEEE Trans. Power Syst.* **2016**, *31*, 3414–3423. [CrossRef]
4. *NB/T31003-2011*; Technical Code for Grid Connected Design of Large Wind Farms. Energy Industry Standard. China Power Engineering Consulting Group Corporation: Beijing, China, 2011.
5. *GB/T31997-2017*; Regulations for Acceptance of Construction Projects of Wind Farms, China. 2019. Available online: https://books.google.co.th/books?id=ghrVAwAAQBAJ&pg=PA1223&lpg=PA1223&dq=Regulations+for+Acceptance+of+Construction+Projects+of+Wind+Farms+GB/T31997-2017&source=bl&ots=9RHMPtNOaS&sig=ACfU3U263EbfA935mH65KCBhLrChk585iA&hl=en&sa=X&ved=2ahUKEwiOl57x5ef-AhUZ1TgGHUYzAIoQ6AF6BAgpEAM#v=onepage&q=Regulations%20for%20Acceptance%20of%20Construction%20Projects%20of%20Wind%20Farms%20GB%2FT31997-2017&f=false (accessed on 17 December 2022).
6. Kumar, D.; Chatterjee, K. A review of conventional and advanced MPPT algorithms for wind energy systems. *Renew. Sustain. Energy Rev.* **2016**, *55*, 957–970. [CrossRef]
7. Zhao, J.J.; Lyu, X.; Fu, Y. Coordinated Microgrid Frequency Regulation Based on DFIG Variable Coefficient Using Virtual Inertia and Primary Frequency Control. *IEEE Trans. Energy Convers.* **2016**, *31*, 833–845. [CrossRef]
8. D'laz-Gonzalez, F.; Bianchi, F.D.; Sumper, A.; Gomis-Bellmunt, O. Control of a flywheel energy storage system for power smoothing in wind power plants. *IEEE Trans. Energy Convers.* **2014**, *29*, 204–214. [CrossRef]
9. Ekanayake, J.; Jenkins, N. Comparison of the response of doubly fed and fixed-speed induction generator wind turbines to changes in network frequency. *IEEE Trans. Energy Convers.* **2004**, *19*, 800–802. [CrossRef]
10. Morren, J.; Pierik, J.; De Haan, S.W. Inertial response of variable speed wind turbines. *Electr. Power Syst. Res.* **2006**, *76*, 980–987. [CrossRef]
11. Lee, J.; Muljadi, E.; Srensen, P.; Kang, Y.C. Releasable Kinetic Energy-Based Inertial Control of a DFIG Wind Power Plant. *IEEE Trans. Sustain. Energy* **2016**, *7*, 279–288. [CrossRef]
12. Li, T.; Wang, L.; Wang, Y.; Liu, G.; Zhu, Z.; Zhang, Y.; Zhao, L.; Ji, Z. Data-Driven Virtual Inertia Control Method of Doubly Fed Wind Turbine. *Energies* **2021**, *14*, 5572. [CrossRef]
13. Liu, J.; Yao, W.; Wen, J.; Liu, Y.; Rui, M.A. Prospect of technology for large-scale wind farm participating into power grid frequency regulation. *Power Syst. Technol.* **2014**, *38*, 638–646.
14. Zhang, X.Y.; Wang, Y.; Fu, Y.; Xu, L. A novel method for obtaining virtual inertia response of DFIG-based wind turbines. *Wind Energy* **2016**, *19*, 313–328. [CrossRef]
15. Liu, J.; Yao, W.; Wen, J.; Ai, X.; Huang, Y. A wind farm virtual inertia compensation strategy based on energy storage system. *Proc. CSEE* **2015**, *35*, 1596–1605.
16. Athari, M.H.; Ardehali, M.M. Operational Performance of Energy Storage as Function of Eelectricity Prices for On-grid Hybrid Renewable Energy System by Optimized Fuzzy Logic Controller. *Renew. Energy* **2016**, *85*, 890–902. [CrossRef]
17. Liu, F.L.W.; Mei, S.W.; Wei, W. ESO-based Inertia Emulation and Rotor Speed Recovery for DFIGs. *IEEE Trans. Energy Convers.* **2017**, *32*, 1209–1219. [CrossRef]

18. Li, X.; Sun, Y.; Su, M.; Wang, H. Coordinated control for unbalanced operation of stand-alone doubly fed induction generator. *Wind. Energy* **2014**, *17*, 317–336. [CrossRef]
19. Jia, F.; Cai, X.; Li, Z. Frequency-distinct control of wind energy conversion system featuring smooth and productive power output. *IEEE Access* **2018**, *6*, 16746–16754. [CrossRef]
20. Zhu, J.; Hu, J.B.; Hung, W.; Wang, C.S. Synthetic Inertia Control Strategy for Doubly Fed Induction Generator Wind Turbine Generators Using Lithium-Ion Supercapacitors. *IEEE Trans. Energy Convers.* **2018**, *33*, 773–783. [CrossRef]